Solid State Sciences 39 (2015) 15–22

Contents lists available at ScienceDirect

Solid State Sciences

journal homepage: www.elsevier.com/locate/ssscie

The germanides Sc*T*Ge (T = Co, Ni, Cu, Ru, Rh, Pd, Ag, Ir, Pt, Au) – Structure and ^{45}Sc solid state NMR spectroscopy

Birgit Heying [a, 1], Sandra Haverkamp [b, 1], Ute Ch Rodewald [a], Hellmut Eckert [b, *], Sebastian C. Peter [c], Rainer Pöttgen [a, *]

[a] Institut für Anorganische und Analytische Chemie, Universität Münster, Corrensstrasse 30, D-48149 Münster, Germany
[b] Institut für Physikalische Chemie, Universität Münster, Corrensstrasse 30, D-48149 Münster, Germany
[c] New Chemistry Unit, Jawaharlal Nehru Centre for Advanced Scientific Research, Jakkur, Bangalore 560064, India

ARTICLE INFO

Article history:
Received 12 September 2014
Received in revised form
21 October 2014
Accepted 10 November 2014
Available online 11 November 2014

Keywords:
Sc*T*Ge germanides
Crystal structure
^{45}Sc solid state NMR spectroscopy

ABSTRACT

The germanides Sc*T*Ge (T = Co, Ni, Cu, Ru, Rh, Pd, Ag, Ir, Pt, Au) were obtained in X-ray pure form by arc-melting of the elements. The structures of the members with T = Co, Ni, Cu, Rh, Pd, Ag, Ir, and Pt were refined on the basis of single crystal X-ray diffractometer data. The germanides with T = Cu, Ru, Pd, Ag crystallize with the hexagonal ZrNiAl type structure, space group $P\bar{6}2m$ and those with T = Co, Ni, Rh, Ir, Pt adopt the orthorhombic TiNiSi type. ScAuGe is isotypic with NdPtSb. All germanides exhibit single scandium sites. A simple systematization of the structure type according to the valence electron concentration is not possible. The ^{45}Sc solid state NMR parameters (Knight shifts and nuclear electric quadrupole coupling constants) of those members crystallizing in the TiNiSi structure show systematic trends as a function of valence electron concentration number. Furthermore, within each *T*-group the Knight shift decreases with increasing atomic number; this correlation also includes previously published results on the isotypic silicide family. The ^{45}Sc quadrupolar interaction tensor components are generally well-reproduced by quantum mechanical electric field gradient calculations using the WIEN2k code.

1. Introduction

The equiatomic silicides Sc*T*Si (T = Co, Ni, Cu, Ru, Rh, Pd, Ir, Pt, Au) [1,2] and Sc*T*Sn (T = Ni, Cu, Pd, Ag, Pt, Au) [3–6] have intensively been studied by ^{45}Sc solid state NMR spectroscopy [7] as a complementary tool to X-ray diffractions. Although both series cover a large number of representatives, an easy systematization of the experimental NMR spectroscopic data is not straightforward. For the silicides [2] both the electric field gradients and the isotropic magnetic shifts decrease with increasing valence electron concentration and within each *T* group the isotropic magnetic shift decreases monotonically with increasing atomic number. In the present study we extended our work to the series of equiatomic germanides Sc*T*Ge with T = Co, Ni, Cu, Ru, Rh, Pd, Ag, Os, Ir, Pt, Au (Table 1). Most of these phases had only been studied on the basis of powder X-ray diffraction [8–14]. High quality single crystal data have only been reported for ScRuGe [12] and ScAuGe [14]. Herein we report structural data for the whole series of Sc*T*Ge germanides. Our studies rely on a combination of X-ray single diffraction data along with ^{45}Sc solid state NMR spectroscopy in order to enlarge the data base for ^{45}Sc nuclear magnetic resonance interaction parameters to understand the relationship between structure and electronic properties.

2. Experimental

2.1. Synthesis

Starting materials for the preparation of the Sc*T*Ge samples were pieces of scandium chips (smart elements), cobalt pieces (Alfa Aesar), nickel wire (Alfa Aesar), copper shot (Chempur, 2–6 mm), ruthenium, rhodium and iridium powder (Agosi), palladium and silver sheet (Agosi), platinum sponge (Agosi), gold granules (Agosi),

* Corresponding authors. Institut für Anorganische und Analytische Chemie and Institut für Physikalische Chemie, Universität Münster, Corrensstrasse 30, D-48149 Münster, Germany.
E-mail addresses: eckerth@uni-muenster.de (H. Eckert), sebastiancp@jncasr.ac.in (S.C. Peter), pottgen@uni-muenster.de (R. Pöttgen).
[1] These authors contributed equally.

http://dx.doi.org/10.1016/j.solidstatesciences.2014.11.001
1293-2558/

Table 1
Lattice parameters and structure types of the equiatomic germanides Sc*T*Ge.

Compound	Structure type	*a*/pm	*b*/pm	*c*/pm	*V*/nm^3	Reference
ScMnGe	ZrNiAl	667.7(1)	*a*	394.6(1)	0.1524	[8]
ScFeGe	ZrNiAl	654.7(1)	*a*	389.5(1)	0.1446	[8]
ScCoGe	TiNiSi	648.2(3)	404.8(1)	707.8(3)	0.1857	this work
ScCoGe	TiNiSi	649.5(6)	400.0(2)	707.2(6)	0.1837	[8]
ScCoGe	TiNiSi	648.1(1)	404.7(1)	708.3(1)	0.1858	[9]
ScNiGe	TiNiSi	645.6(1)	407.6(1)	708.3(2)	0.1864	this work
ScNiGe	TiNiSi	645.4(6)	407.1(3)	706.8(7)	0.1857	[8]
ScCuGe	ZrNiAl	651.8(2)	*a*	397.2(1)	0.1461	this work
ScCuGe	ZrNiAl	651.0(2)	*a*	399.8(2)	0.1467	[8]
ScCuGe	ZrNiAl	651.4(1)	*a*	397.2(1)	0.1460	[10]
ScCuGe	ZrNiAl	651.5(1)	*a*	397.2(1)	0.1460	[11]
ScRuGe	ZrNiAl	694.8(3)	*a*	346.5(1)	0.1448	this work
ScRuGe	ZrNiAl	696.2(1)	*a*	346.83(9)	0.1456	[12]
ScRhGe	ZrNiAl	667.2(2)	*a*	379.4(2)	0.1463	[12]
ScRhGe	TiNiSi	649.7(7)	411.2(5)	738.5(7)	0.1973	[12]
ScRhGe	TiNiSi	651.1(1)	412.00(6)	740.42(9)	0.1986	this work
ScPdGe	ZrNiAl	670.8(1)	*a*	392.50(6)	0.1529	this work
ScPdGe	ZrNiAl	671.53(7)	*a*	392.50(6)	0.1533	[12]
ScAgGe	ZrNiAl	686.51(4)	*a*	402.95(3)	0.1645	this work
ScAgGe	ZrNiAl	688.2(2)	*a*	402.6(1)	0.1651	[13]
ScOsGe	ZrNiAl	692.8(1)	*a*	346.7(1)	0.1441	[12]
ScIrGe	TiNiSi	645.33(7)	411.54(7)	748.0(1)	0.1987	this work
ScIrGe	TiNiSi	644.6(4)	410.7(3)	748.2(4)	0.1981	[12]
ScPtGe	TiNiSi	658.91(8)	421.43(6)	741.4(1)	0.2059	this work
ScPtGe	TiNiSi	658.5(1)	421.5(1)	741.4(1)	0.2058	[12]
ScAuGe	NdPtSb	430.8(1)	*a*	684.7(1)	0.1100	this work
ScAuGe	NdPtSb	430.82(5)	*a*	684.58(10)	0.1100	[14]

and germanium granules (Chempur), all with stated purities > 99.9%. Pieces of the three elements were mixed in the ideal 1: 1: 1 atomic ratio and arc-melted [15] under an argon pressure of ca. 800 mbar. The argon was purified over titanium sponge (900 K), silica gel and molecular sieves. The powdered elements were first cold-pressed to pellets. The product buttons were re-melted several times to ensure homogeneity. The total weight-losses after several meltings were smaller than 0.5%. The brittle samples have metallic luster and are stable in air over weeks.

Except for ScAgGe all samples were obtained in X-ray pure form directly after arc-melting. The arc-melted ScAgGe button was sealed in an evacuated silica tube and annealed at 970 K in a muffle furnace for one week followed by quenching.

2.2. EDX data

Semiquantitative EDX analyses of the Sc*T*Ge crystals investigated on the diffractometers were carried out by use of a Zeiss EVO® MA10 scanning electron microscope in variable pressure mode with scandium, the elemental transition metals and germanium as standards. The experimentally observed compositions were all close to the ideal ones. No impurity elements were observed.

2.3. X-ray diffraction

First analyses of the Sc*T*Ge samples was done by powder X-ray diffraction through Guinier patterns using Cu$K_{\alpha1}$ radiation and α-quartz ($a = 491.30$ and $c = 540.46$ pm) as an internal standard. The Guinier camera was equipped with an imaging plate technique (Fuji film, BAS-READER 1800). The lattice parameters (Table 1) were obtained from least-squares refinements. Correct indexing of the patterns was ensured through intensity calculations [16].

Small single crystals of the Sc*T*Ge germanides were isolated from the crushed arc-melted samples. They were glued to thin quartz fibers and investigated on a Buerger precession camera (white Mo radiation, Fuji-film imaging plate) in order to check their quality for intensity data collection. Most data sets were collected at room temperature by using a Stoe IPDS-II image plate system (graphite monochromatized Mo radiation; $\lambda = 71.073$ pm) in oscillation mode. Numerical absorption corrections were applied to the data sets. The ScAgGe crystal was measured at room temperature using a four-circle diffractometer (CAD4) with graphite monochromatized AgK_α radiation ($\lambda = 56.087$ pm) and a scintillation counter with pulse height discrimination. Scans were taken in the $\omega/2\theta$ mode. An absorption correction was based on psi-scans. Details on the crystallographic data are given in Tables 2 and 3.

2.4. Solid state NMR spectroscopy

Room temperature solid state ^{45}Sc NMR studies were carried out at 121.54, 72.92 and 48.59 MHz using Bruker DSX 500, BRUKER Avance III-300 and Bruker DSX-200 spectrometers. Powdered materials diluted with silica in 1:1 ratio by weight were examined within 2.5 mm zirconia rotors under magic-angle spinning (MAS) conditions using a spinning frequency of 25.0 kHz Wide-band single pulse excitation was accomplished with short hard pulses of typically 0.5 μs length, corresponding to 30° flip angles on solid samples and relaxation delays of 1s. NMR interaction parameters were extracted from the spectra using the DMFIT software [17]. Isotropic magnetic shifts are referenced against 1 M aqueous $ScCl_3$ solution.

Theoretical electric field gradient calculations were conducted using the WIEN2k code, a full-potential all electron method based on the LAPW + LO method [18]. SCF calculations were done with R_{mt} parameters of 2.5 for Sc, 2.24–2.49 for the *T*-atoms, and 2.13–2.34 atomic units for Ge. Separation energies between the core and valence states were set to −6 Ry. The plane wave cutoff parameter $R_{mt}^{min} \times K_{max}$ was optimized in steps of 0.5 units within the range of 5.50–7.00. For ScAuGe a value of 5.50 was used, while for all the other compounds it was 7.00. For describing the first Brillouin zone, 3 k-points were used initially, and this was

Table 2
Crystal data and structure refinement results for Sc*T*Ge (*T* = Co, Ni, Cu and Rh).

Compound	ScCoGe	ScNiGe	ScCuGe	ScRhGe
Structure type	TiNiSi	TiNiSi	ZrNiAl	TiNiSi
Space group	*Pnma*	*Pnma*	$P\bar{6}2m$	*Pnma*
Formula units, *Z*	4	4	3	4
Molar mass, g mol^{-1}	176.48	176.26	181.09	220.46
Calculated density, g cm^{-3}	6.31	6.28	6.17	7.37
Absorption coefficient, mm^{-1}	27.9	29.0	29.0	26.0
F(000), e	320	324	246	392
Crystal size, μm^3	20 × 40 × 80	20 × 20 × 50	30 × 40 × 60	20 × 40 × 60
Transm. ratio (min/max)	0.188/0.539	0.322/0.689	0.365/0.500	0.300/0.549
θ range, deg	4–35	4–35	3–32	4–35
Range in *hkl*	±10, ±6, ±11	±10, ±6, ±11	±9, ±9, ±5	±10, ±6, ±11
Total no. reflections	2355	2213	1474	2361
Independent reflections/R_{int}	454/0.0258	458/0.0499	215/0.0451	480/0.0529
Reflections with $I \geq 2\sigma(I)/R_\sigma$	423/0.0137	351/0.0335	204/0.0218	412/0.0318
Data/parameters	454/20	458/20	215/15	480/20
Goodness-of-fit on F^2	1.118	0.955	1.176	0.970
*R*1/*wR*2 for $I \geq 2\sigma(I)$	0.0142/0.0241	0.0223/0.0367	0.0272/0.0625	0.0192/0.0365
*R*1/*wR*2 for all data	0.0165/0.0245	0.0392/0.0391	0.0305/0.0635	0.0282/0.0383
Extinction coefficient	0.0160(10)	0.0086(8)	0.006(3)	0.0108(8)
BASF	–	–	0.48(6)	–
Largest diff. peak/hole, e Å^{-3}	0.77/− 0.88	1.31/− 1.24	1.61/− 0.83	1.02/− 1.75

Table 3
Crystal data and structure refinement results for Sc*T*Ge (T = Pd, Ag, Ir and Pt).

Compound	ScPdGe	ScAgGe	ScIrGe	ScPtGe
Structure type	ZrNiAl	ZrNiAl	TiNiSi	TiNiSi
Space group	$P\bar{6}2m$	$P\bar{6}2m$	*Pnma*	*Pnma*
Formula units, Z	3	3	4	4
Molar mass, g mol^{-1}	223.95	225.42	309.75	312.64
Calculated density, g cm^{-3}	7.29	6.83	10.36	10.09
Absorption coefficient, mm^{-1}	26.1	13.1	84.7	85.0
F(000), e	297	300	520	524
Crystal size, μm^3	30 × 40 × 60	20 × 20 × 40	10 × 20 × 80	20 × 30 × 40
Transm. ratio (min/max)	0.317/0.500	0.246/0.558	0.058/0.285	0.152/0.452
θ range, deg	3–35	2–24	4–35	4–35
Range in hkl	±10, ±10, ±6	+9, ±9, ±5	±10, ±6, ±11	±10, ±6, ±11
Total no. reflections	2527	1111	3022	2732
Independent reflections/R_{int}	284/0.0303	216/0.0655	480/0.0631	496/0.0318
Reflections with $I \geq 2\sigma(I)/R_\sigma$	281/0.0170	205/0.0372	429/0.0327	455/0.0189
Data/parameters	284/14	216/14	480/20	496/20
Goodness-of-fit on F^2	1.254	1.133	0.932	1.005
$R1/wR2$ for $I \geq 2\sigma(I)$	0.0131/0.0195	0.0255/0.0514	0.0170/0.0250	0.0143/0.0246
$R1/wR2$ for all data	0.0133/0.0195	0.0285/0.0531	0.0237/0.0258	0.0169/0.0249
Extinction coefficient	0.239(6)	0.034(4)	0.00422(15)	0.0065(3)
Flack Parameter	−0.026(11)	0.10(7)	–	–
Largest diff. peak/hole, e Å^{-3}	0.63/−1.54	0.95/−0.92	1.81/−2.65	2.10/−1.49

Table 4
Atomic coordinates and isotropic displacement parameters (pm^2) of Sc*T*Ge (T = Co, Ni, Cu, Rh, Pd, Ag, Ir and Pt). U_{eq} is defined as one third of the trace of the orthogonalized U_{ij} tensor.

Atom	Wyckoff position	x	y	z	U_{eq}
ScCoGe (*Pnma*)					
Sc	4*c*	−0.00005(5)	1/4	0.69879(5)	51(1)
Co	4*c*	0.15537(4)	1/4	0.06092(4)	48(1)
Ge	4*c*	0.28444(3)	1/4	0.39032(3)	44(1)
ScNiGe (*Pnma*)					
Sc	4*c*	−0.00393(13)	1/4	0.70694(9)	52(1)
Ni	4*c*	0.18687(7)	1/4	0.07816(7)	65(1)
Ge	4*c*	0.29296(6)	1/4	0.40640(6)	48(1)
ScCuGe ($P\bar{6}2m$)					
Sc	3*f*	0.5714(4)	0	0	93(4)
Cu	3*g*	0.2425(2)	0	1/2	115(3)
Ge1	2*d*	2/3	1/3	1/2	75(3)
Ge2	1*a*	0	0	0	98(4)
ScRhGe (*Pnma*)					
Sc	4*c*	0.01286(13)	1/4	0.69405(11)	57(1)
Rh	4*c*	0.15765(5)	1/4	0.06106(4)	43(1)
Ge	4*c*	0.27877(7)	1/4	0.38506(6)	48(1)
ScPdGe ($P\bar{6}2m$)					
Sc	3*f*	0.42318(10)	0	0	70(1)
Pd	3*g*	0.75151(3)	0	1/2	90(1)
Ge1	2*d*	1/3	2/3	1/2	54(1)
Ge2	1*a*	0	0	0	97(1)
ScAgGe ($P\bar{6}2m$)					
Sc	3*f*	0.5821(4)	0	0	58(5)
Ag	3*g*	0.2526(1)	0	1/2	81(2)
Ge1	2*d*	1/3	2/3	1/2	59(3)
Ge2	1*a*	0	0	0	75(5)
ScIrGe (*Pnma*)					
Sc	4*c*	0.01661(17)	1/4	0.68795(14)	61(2)
Ir	4*c*	0.16274(3)	1/4	0.05656(3)	46(1)
Ge	4*c*	0.28186(9)	1/4	0.37677(8)	51(1)
ScPtGe (*Pnma*)					
Sc	4*c*	−0.00082(13)	1/4	0.70472(12)	55(1)
Pt	4*c*	0.20489(2)	1/4	0.08269(2)	51(1)
Ge	4*c*	0.30230(7)	1/4	0.40754(6)	54(1)

successively increased up to 400 k-points. 2238-5635 plane waves were used to describe the electronic state of the crystal structures. The calculations were done based on the exact crystallographic output data and no structural relaxation was performed.

3. Results and discussion

3.1. Structure refinements

Analyses of the eight data sets either revealed hexagonal or primitive orthorhombic lattices and the systematic extinctions were compatible with space groups $P\bar{6}2m$ or *Pnma*, in agreement with our earlier studies on the related silicide series [2]. The atomic positions of ScCoSi [2] and ScRuGe [12] were taken as starting values and the structures were refined with anisotropic displacement parameters for all atoms with Shelxl-97 (full-matrix least-squares on F_o^2) [19]. To check for deviations from the ideal composition, the occupancy parameters were refined in separate series of least-squares cycles. All sites were fully occupied within three standard deviations. The final difference Fourier synthesis revealed no significant residual densities. The atomic coordinates and interatomic distances (exemplarily for ScPdGe and ScCoGe) are listed in Tables 4 and 5. Refinement of the correct absolute structure for the non-centrosymmetric ZrNiAl type germanides was ensured through calculation of the Flack parameter [20,21]. Only the ScCuGe data set was refined as an inversion twin (Table 2).

Further details of the structure refinements may be obtained from the Fachinformationszentrum Karlsruhe, D-76344 Eggenstein-Leopoldshafen (Germany), by quoting the Registry No's. CSD−428472 (ScCoGe), CSD−428471 (ScNiGe), CSD−428473 (ScCuGe), CSD−428475 (ScRhGe), CSD−428470 (ScPdGe), CSD−428469 (ScAgGe), CSD−428468 (ScIrGe), and CSD−428474 (ScPtGe).

3.2. Crystal chemistry

The Sc*T*Ge germanides adopt two different structure types, either the orthorhombic TiNiSi (space group *Pnma* [22]) or the

Table 5
Interatomic distances (pm), calculated with the powder lattice parameters of ScPdGe (ZrNiAl-type) and ScCoGe (TiNiSi-type). All distances within the first coordination spheres are listed. Standard deviations are all equal or less than 0.1 pm.

ScPdGe				ScCoGe			
Sc:	4	Ge1	280.5	Sc:	1	Co	275.4
	1	Ge2	283.9		2	Ge	280.8
	2	Pd	295.0		2	Ge	280.9
	4	Pd	315.5		2	Co	282.9
Pd:	2	Ge1	256.8		1	Ge	285.8
	2	Ge2	257.5		1	Co	289.3
	2	Pd	288.7		2	Co	316.9
	2	Sc	295.0		1	Ge	322.6
	4	Sc	315.5	Co:	2	Ge	238.9
Ge1:	3	Pd	256.8		1	Ge	242.9
	6	Sc	280.5		1	Ge	247.7
Ge2:	6	Pd	257.5		1	Sc	275.4
	3	Sc	283.9		2	Sc	282.9
					1	Sc	289.3
					2	Co	298.3
					2	Sc	316.9
				Ge:	2	Co	238.9
					1	Co	242.9
					1	Co	247.7
					2	Sc	280.8
					2	Sc	280.9
					1	Sc	285.8
					1	Sc	322.6

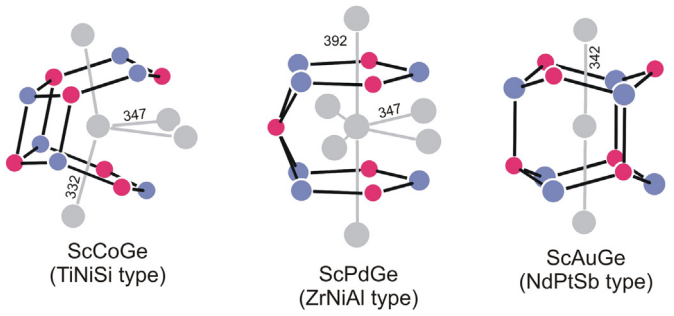

Fig. 1. Coordination of the scandium atoms in the structures of ScCoGe, ScPdGe, and ScAuGe. Scandium, transition metal, and germanium atoms are drawn as light gray, blue, and magenta circles, respectively. The transition metal-germanium polyanionic networks and relevant Sc–Sc distances are indicated. (For interpretation of the references to color in this figure legend, the reader is referred to the web version of this article.)

hexagonal ZrNiAl (space group $P\bar{6}2m$ [23–25]) type structure. These are two prominent structure types for equiatomic intermetallic compounds [26]. Only ScAuGe [14] is an exception. It crystallizes with the NdPtSb type, an AlB_2 superstructure with puckered Au_3Ge_3 hexagons. A view on Table 1 readily shows that formation of one of these types is not a simple function of the group or period number. Also comparisons with the corresponding equiatomic silicides Sc*T*Si [2] and the stannides Sc*T*Sn [3–6] are not simple. While the silicides crystallize in the TiNiSi structure without exception, the stannides crystallize within five different structure types. In the Sc*T*Ge family three distinct structure types are realized. To highlight their difference we will in the following exemplarily discuss the near-neighbor coordination of the scandium atoms in ScPdGe (ZrNiAl type), ScCoGe (TiNiSi type), and ScAuGe (NdPtSb type). For a broader crystal chemical discussion on the respective prototypes we refer to review articles [27–31].

The scandium near-neighbor coordinations of the three exemplary germanides are shown in Fig. 1. The puckered Co_3Ge_3 and Au_3Ge_3 hexagons which coordinate the scandium atoms in ScCoGe and ScAuGe are readily visible. The *T*–Ge distances are always on the order of the sums of the covalent radii [32], indicating substantial *T*–Ge bonding. The polyanion of ScPdGe with ZrNiAl type structure is slightly different. The scandium atoms are coordinated by two planar but slightly distorted Pd_3Ge_2 pentagons which are condensed by another germanium atom. These three different types of polyanions lead to three types of scandium arrangements. In ScAuGe the nearest scandium neighbors are along the *c* axis with Sc–Sc distances of 342 pm. The next nearest scandium atoms within this hexagonal structure (space group $P6_3mc$) are at 431 pm which corresponds to the *a* lattice parameter. This Sc–Sc distance is much longer than in elemental hexagonal scandium (6×325 and 6×331 pm) [33].

In the TiNiSi and ZrNiAl type phases we observe more Sc–Sc nearest neighbor interactions. The strong puckering of the Co_3Ge_3 hexagons in ScCoGe leaves only space for two scandium neighbors between the hexagons. The corresponding Sc–Sc distances of 332 and 347 pm are similar to the short one in ScAuGe. The largest number of scandium neighbors occurs in ScPdGe. The six scandium atoms are at Sc–Sc distances of 347 and 392 pm. Again, the four shorter ones compare well with ScCoGe and ScAuGe. In the following section we discuss these structural peculiarities based on the ^{45}Sc solid state NMR spectra.

3.3. ^{45}Sc solid state NMR spectroscopy

Figs. 2–4 summarize the solid state NMR spectra. In all cases an intense central peak, corresponding to the $m = 1/2 \Leftrightarrow m = -1/2$ Zeeman transition is observed, which is flanked by a set of multiple spinning sidebands originating from the six $m = \pm 1/2 \Leftrightarrow m = \pm 3/2$, $m = \pm 3/2 \Leftrightarrow m = \pm 5/2$ and $m = \pm 5/2 \Leftrightarrow m = \pm 7/2$ Zeeman

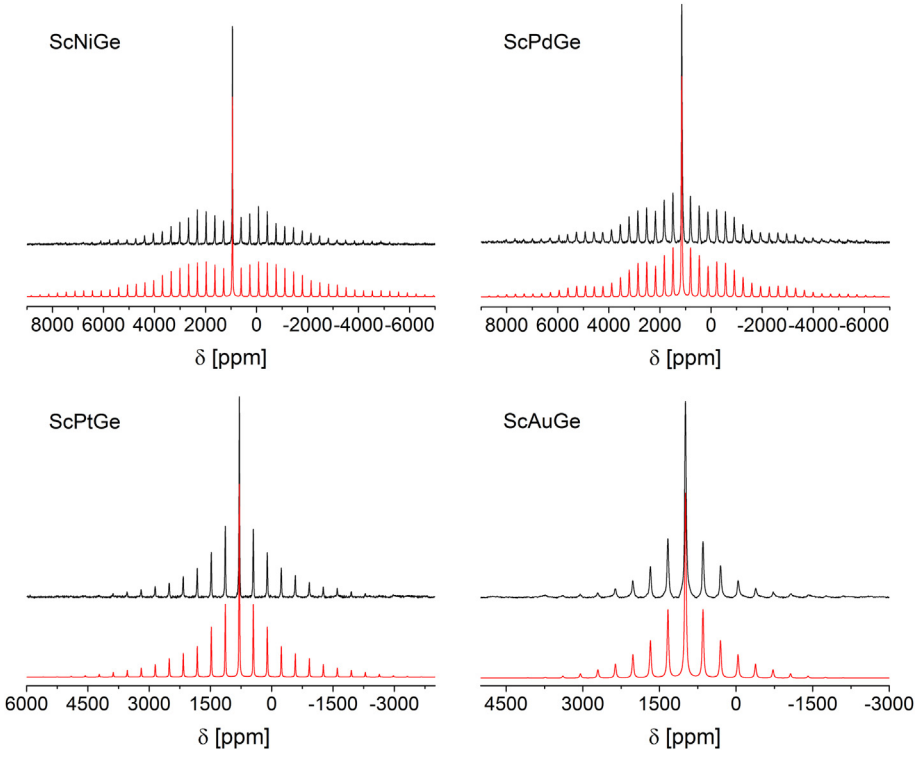

Fig. 2. Experimental (top) and simulated (bottom) ^{45}Sc MAS-NMR spectra of ScNiGe, ScPdGe, ScPtGe and ScAuGe.

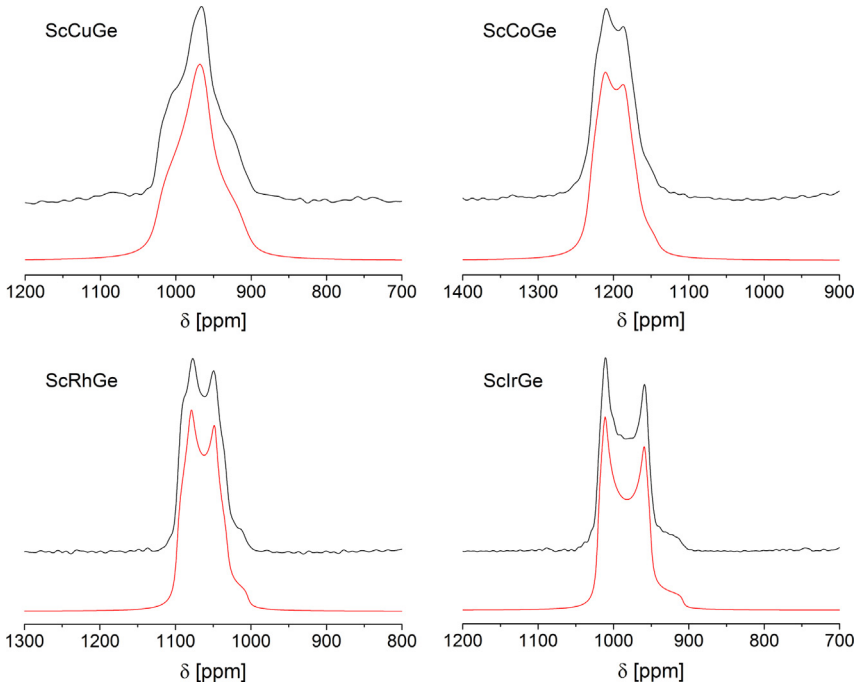

Fig. 3. Experimental (top) and simulated (bottom) ^{45}Sc MAS-NMR spectra of ScCuGe, ScCoGe, ScRhGe and ScIrGe.

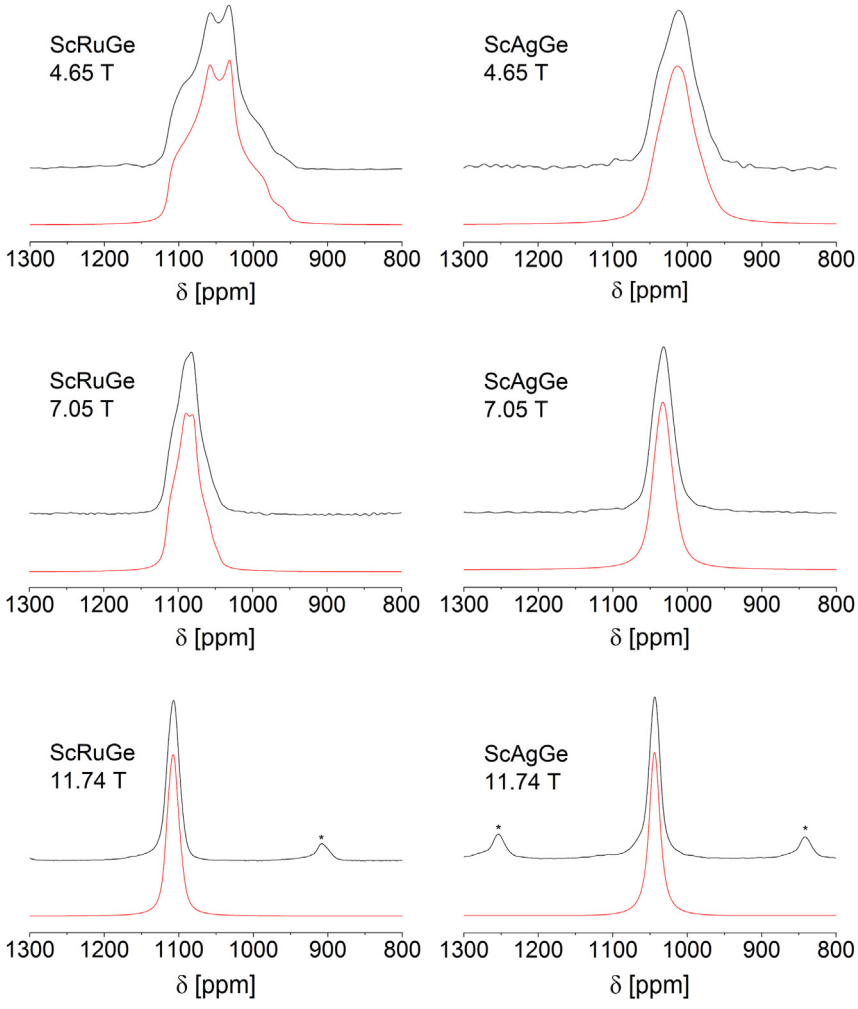

Fig. 4. Field dependent experimental (top) and simulated (bottom) ^{45}Sc MAS-NMR spectra of ScRuGe and ScAgGe.

transitions ($\Delta m = \pm 1$). In contrast to the sharp central transition, these six "satellite" transitions are anisotropically broadened by the nuclear electric quadrupolar interactions in the limit of first-order perturbation theory. Under magic-angle spinning conditions at slow-spinning speeds ($\omega_r << C_Q$) incomplete coherent averaging is observed, resulting in the appearance of wide spinning sideband patterns whose intensity distribution forms the envelope of the powder pattern. The relevant parameters characterizing the quadrupole interaction are the nuclear electric quadrupolar coupling constant $C_Q (= e^2qQ/h$, i.e. the product of the nuclear electric quadrupole moment eQ and the maximum electric field gradient component eq_{zz}, divided by Planck's constant) and the electric field gradient asymmetry parameter $\eta_Q = (eq_{xx} - eq_{yy})/eq_{zz}$, which characterizes the deviation of the electric field gradient from cylindrical symmetry. These parameters were extracted from this spinning sideband pattern via visual comparison with simulations.

Fig. 2 shows typical examples for those compounds in which the quadrupolar coupling is relatively weak. In the spectra of those compounds with stronger quadrupolar coupling ($C_Q > 4$ MHz) the sideband pattern becomes too wide to be observable within the bandwidths of the NMR probes utilized, resulting in an attenuation of the outer spinning sidebands at large resonance offsets owing to incomplete excitation. In this regime, more accurate quadrupole coupling information can be obtained by analyzing the line shape of the central transition, which is affected by second-order quadrupolar perturbation. Fig. 3 summarizes typical results obtained for those compounds having quadrupolar coupling constants >7 MHz. In the intermediate regime, 4MHz < C_Q < 7 MHz, the structured line shape predicted from these second-order effects may not always be clearly apparent. In this case, the central transition line shape analysis needs to be augmented by careful field-dependent line shape studies. Fig. 4 shows two typical examples of the present study. Table 6 summarizes all the information obtained from the NMR data.

In general, the experimental C_Q values are found in excellent agreement with those calculated theoretically using the WIEN2k code (see Fig. 5a). Good agreement is also observed for most of the asymmetry parameters (Fig. 5b), with the exception of the compounds ScAuGe and ScPtGe. We attribute this discrepancy to a large experimental uncertainty with which the quadrupolar coupling constants can be obtained from the spinning sideband intensity profiles in this case. Further listed in Table 6 are the isotropic magnetic shifts obtained relative to the 1 M $ScCl_3$ solution reference standard. The resonance frequencies in these compounds are dominated by Knight shifts, which are caused by the probability density of unpaired conduction electron density near the Fermi edge at the ^{45}Sc nuclei. Although to the present date, no reliable

Table 6
Isotropic magnetic shifts δ_{iso} (±2 ppm), nuclear electric quadrupolar coupling constant C_Q (±0.05 MHz), electric field gradient asymmetry parameter η_Q (±0.05) of Sc*T*Ge compounds. For C_Q and η_Q both experimental and theoretically calculated values are listed.

Compound	δ_{iso} [ppm]	C_Q [MHz]	C_Q^{theo} [MHz]	η_Q	η_Q^{theo}
ScCoGe	1236	8.76	9.58	0.36	0.38
ScRhGe	1103	9.04	9.21	0.33	0.30
ScIrGe	1034	10.25	10.48	0.13	0.15
ScNiGe	951	3.14	3.69	0.00	0.02
ScPtGe	798	1.30	1.29	0.97[b]	0.07
ScRuGe	1116	7.50	7.70	0.62	0.62
ScPdGe	1160	2.73	2.00[a]	0.85	0.86[a]
ScCuGe	1124	9.49	8.90	0.84	0.92
ScAgGe	1051	5.56	4.81	0.63	0.71
ScAuGe	1014	0.90	1.13	0.7[b]	0.00

[a] Spin polarized calculation.
[b] Data considered less reliable.

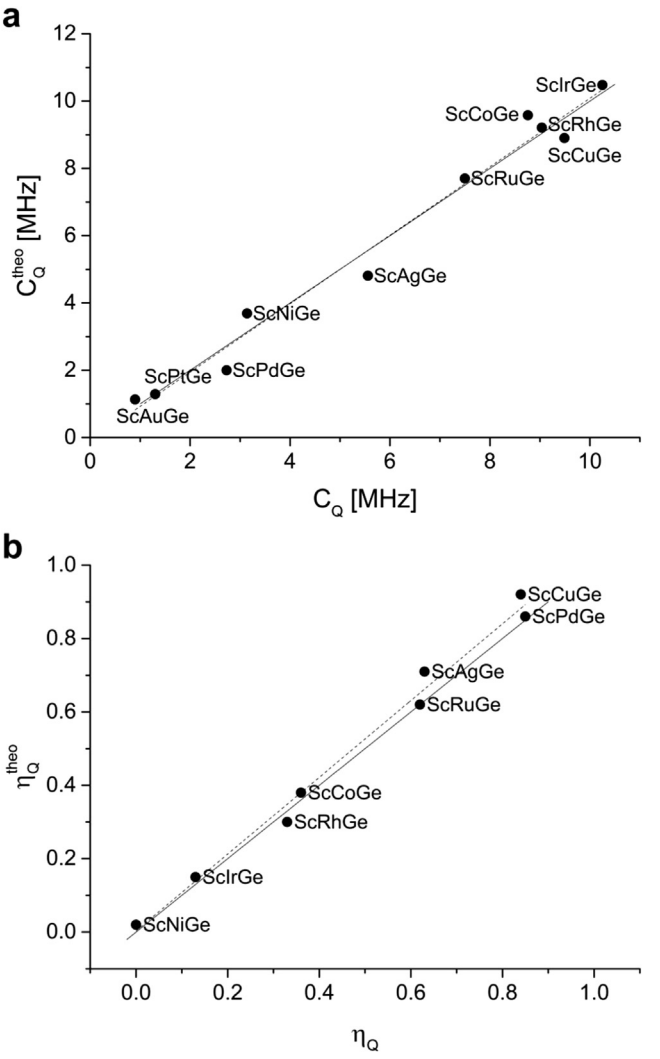

Fig. 5. Comparison of experimental and theoretically calculated C_Q (top) and η_Q values (bottom) for compounds in the series Sc*T*Ge. The solid lines denote the identity, while the dashed lines represent linear least-squares fits to the data.

computational methods exist for predicting Knight shifts theoretically, useful semi-empirical correlations with electronic properties can sometimes be found within series of isotypic compounds. For example, within the Sc*T*Si family crystallizing in the TiNiSi structure, the isotropic shifts were found to decrease monotonically with decreasing atomic number and a systematic dependence on the *T*-group number (i.e. the valence electron concentration) was found [2]. Fig. 6 illustrates that this general trend also includes all those equiatomic Sc*T*Ge compounds of the present series, which crystallize in the TiNiSi structure. In contrast, the isotropic magnetic shifts of the ZrNiAl-type germanides are systematically higher, and do not match this general trend. These results once again reveal that meaningful magnetic shift correlations are only possible within series of isotypic compounds.

Interesting compositional and crystallographic systematics are further apparent for the nuclear electric quadrupolar coupling constants and the asymmetry parameters (see Table 6 and Figs. 7 and 8). The C_Q values show a distinctive dependence on the valence electron concentration (group number), and this dependence encompasses compounds of the TiNiSi structure as well as those of other crystal structures. For compounds with *T* elements of Group-9 C_Q-values near 9–10 MHz are observed, while for

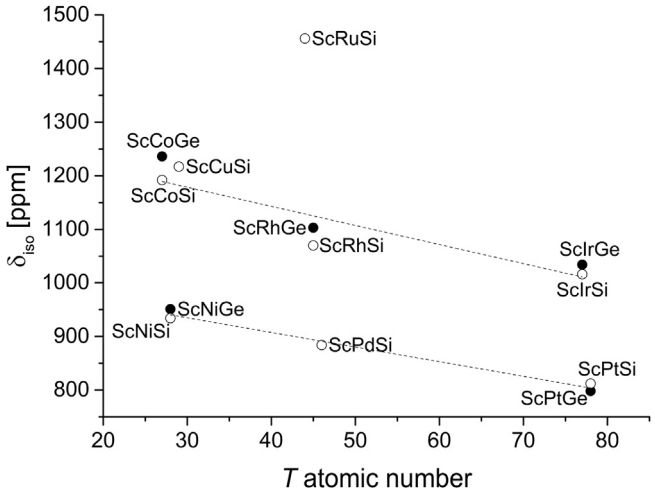

Fig. 6. Correlation of the isotropic magnetic shift in Sc*T*Ge compounds crystallizing in the TiNiSi structure with atomic number and valence electron concentration (group number). Data for the previously examined isotypic Sc*T*Si series are included. The dashed lines are linear least-squares fits to the data referring to compounds of the group 9 and the group 10 *T* atoms, respectively.

compounds with *T*-atoms from group 10, the C_Q values are below 4 MHz. For compounds of group 11, we observe a strong decrease of C_Q with increasing atomic number. Fig. 7 illustrates that both the germanides and the previously investigated silicides follow the same trend. Furthermore, a decisive crystallographic distinction is observed for the asymmetry parameter: In compounds crystallizing in the TiNiSi structure the asymmetry parameters are generally low ($\eta_Q < 0.4$, with a tendency to decrease with increasing atomic number), whereas compounds crystallizing in the ZrNiAl structure have significantly larger asymmetry parameters, $\eta_Q > 0.6$). This behavior indicates that the Sc atoms are found on more strongly distorted sites within the ZrNiAl structure than within the TiNiSi structure.

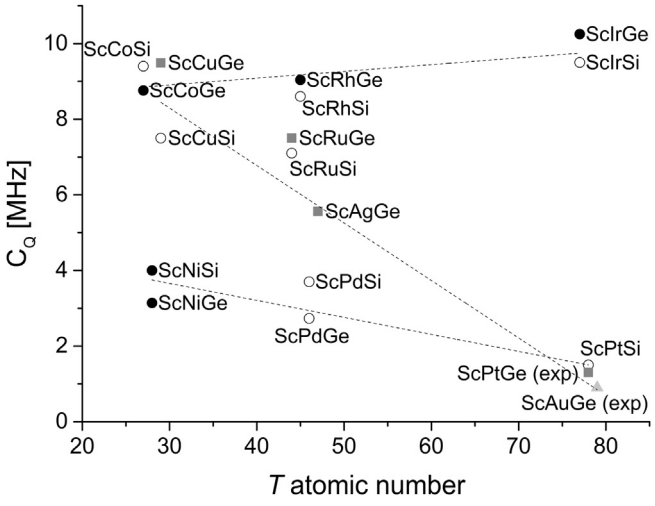

Fig. 7. Correlation of the nuclear electric quadrupolar coupling constants in Sc*T*Ge and Sc*T*Si compounds with atomic number and valence electron concentration (group number). Circles denote compounds crystallizing in the TiNiSi structure, squares denote compounds crystallizing in the ZrNiAl structure, triangles denote the compound crystallizing in the NdPtSb structure. Dashed lines represent linear least-squares fits to the respective data for the compounds having *T* atoms of group 9, group 10 and group 11, respectively.

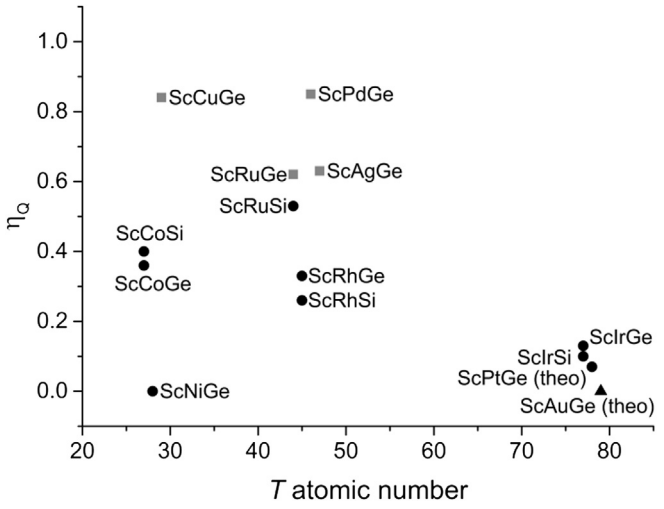

Fig. 8. Correlation of the electric field gradient asymmetry parameter in Sc*T*Ge and Sc*T*Si compounds with atomic number and valence electron concentration (group number). Circles denote compounds crystallizing in the TiNiSi structure, squares denote compounds crystallizing in the ZrNiAl structure, triangles denote the compound crystallizing in the NdPtSb structure. Data points for ScPtGe and ScAuGe stem from the theoretical calculations, as the experimental values have large uncertainties (see text).

4. Conclusions

While compounds of the Sc*T*Si series uniformly crystallize in the TiNiSi structure, the compositionally related germanides form three, and the stannides even five structure types. ^{45}Sc Knight shift and quadrupolar coupling constant trends as a function of composition can be identified within the series of isotypic compounds of the TiNiSi structure type. Systematic trends are observed both as a function of valence electron concentration (group number) and atomic number. In contrast the influence of the group 14 element (Si or Ge) is small, with exception of the Ru compounds. Furthermore, the TiNiSi and ZrNiAl structure types can be clearly differentiated on the basis of nuclear electric quadrupolar coupling constants and electric field gradient asymmetry parameters. Their experimental values are found in excellent agreement with the values determined from quantum chemical calculations.

Acknowledgments

This work was financially supported by the Deutsche Forschungsgemeinschaft.

References

[1] C.P. Sebastian, L. Zhang, H. Eckert, R. Pöttgen, Z. Naturforsch 62b (2007) 173.
[2] T. Harmening, H. Eckert, C.M. Fehse, C.P. Sebastian, R. Pöttgen, J. Solid State Chem. 184 (2011) 3303.
[3] C.P. Sebastian, H. Eckert, S. Rayaprol, R.-D. Hoffmann, R. Pöttgen, Solid State Sci. 8 (2006) 560.
[4] C.P. Sebastian, C. Fehse, H. Eckert, R.-D. Hoffmann, R. Pöttgen, Solid State Sci. 8 (2006) 1386.
[5] C.P. Sebastian, L. Zhang, C. Fehse, R.-D. Hoffmann, H. Eckert, R. Pöttgen, Inorg. Chem. 46 (2007) 771.
[6] T. Harmening, C.P. Sebastian, L. Zhang, C. Fehse, H. Eckert, R. Pöttgen, Solid State Sci. 10 (2008) 1395.
[7] H. Eckert, R. Pöttgen, Z. Anorg. Allg. Chem. 636 (2010) 2232.
[8] R.V. Skolozdra, B.Ya Kotur, R.I. Andrusyak, YuK. Gorelenko, Inorg. Mater. 27 (1991) 1371.
[9] A.E. Dwight, P.P. Vaishnava, C.W. Kimball, J.L. Matykiewicz, J. Less-Common Met. 119 (1986) 319.
[10] A.E. Dwight, Proc. Rare Earth Res. Conf. 7th, vol. 1, 1969, p. 273.
[11] A.E. Dwight, W.C. Harper, C.W. Kimball, J. Less-Common Met. 30 (1973) 1.

[12] E. Hovestreydt, N. Engel, K. Klepp, B. Chabot, E. Parthé, J. Less-Common Met. 85 (1982) 247.
[13] B.Y. Kotur, L.A. Boychuk, Visn. Lviv Derzh. Univ. Ser. Khim 29 (1988) 51.
[14] R. Pöttgen, H. Borrmann, C. Felser, O. Jepsen, R. Henn, R.K. Kremer, A. Simon, J. Alloys Compd. 235 (1996) 170.
[15] R. Pöttgen, T. Gulden, A. Simon, GIT Labor-Fachzeitschrift 43 (1999) 133.
[16] K. Yvon, W. Jeitschko, E. Parthé, J. Appl. Crystallogr. 10 (1977) 73.
[17] D. Massiot, F. Fayon, M. Capron, I. King, S. Le Calvé, B. Alonso, J.-O. Durand, B. Bujoli, Z. Gan, G. Hoatson, Magn. Reson. Chem. 40 (2002) 70.
[18] P. Blaha, K. Schwarz, G.K.H. Madsen, D. Kvasnicka, J. Luitz, in: K.H. Schwarz (Ed.), WIEN2k, An Augmented Plane Wave + Local Orbitals Program for Calculating Crystal Properties, Technical University, Wien Austria, 2001, 3-9501031-2.
[19] G.M. Sheldrick, Acta Crystallogr. A64 (2008) 112.
[20] H.D. Flack, G. Bernadinelli, Acta Crystallogr. A 55 (1999) 908.
[21] H.D. Flack, G. Bernadinelli, J. Appl. Crystallogr. 33 (2000) 1143.
[22] C.B. Shoemaker, D.P. Shoemaker, Acta Crystallogr. 18 (1965) 900.
[23] P.I. Krypyakevich, V.Ya Markiv, E.V. Melnyk, Dopov. Akad. Nauk. Ukr. RSR, Ser. A (1967) 750.
[24] A.E. Dwight, M.H. Mueller, R.A. Conner Jr., J.W. Downey, H. Knott, Trans. Met. Soc. AIME 242 (1968) 2075.
[25] M.F. Zumdick, R.-D. Hoffmann, R. Pöttgen, Z. Naturforsch 54b (1999) 45.
[26] R. Pöttgen, D. Johrendt, Intermetallics – Synthesis, Structure, Function, De Gruyter, Berlin, 2014.
[27] E. Parthé, L. Gelato, B. Chabot, M. Penzo, K. Cenzual, R. Gladyshevskii, TYP-IX–standardized data and crystal chemical characterization of inorganic structure types, in: Gmelin Handbook of Inorganic and Organometallic Chemistry, Springer, Berlin (Germany), 1993.
[28] G.A. Landrum, R. Hoffmann, J. Evers, H. Boysen, Inorg. Chem. 37 (1998) 5754.
[29] M.F. Zumdick, R. Pöttgen, Z. Kristallogr. 214 (1999) 90.
[30] R.-D. Hoffmann, R. Pöttgen, Z. Kristallogr. 216 (2001) 127.
[31] R. Pöttgen, Z. Anorg. Allg. Chem. 640 (2014) 869.
[32] J. Emsley, The Elements, Oxford University Press, 1999.
[33] J. Donohue, The Structures of the Elements, Wiley, New York, 1974.